

## CHAPTER V

### Crawl Gait Results

To test the efficacy of the Projected Profile crawling gait, a gait sequence was generated using MATLAB and simulated using the V-REP simulator by Coppelia Robotics. The crawling sequence was generated using the nominal crawling parameters. The Nao humanoid platform was then programmed using the NaoQI API in C++ to use this sequence to execute a crawling action. The robot was initialized to its crawling pose and placed on the ground where it crawled under a vertically constrained table. During this experiment, the joint angles and joint motor currents were recorded for later analysis. To demonstrate a context under which the gait would be used, the Nao was then programmed to walk to a fiducial marker, position itself into the crawling position, crawl under the vertically constrained table, and then return to a sitting position. NaoQI provides functions for the Nao to walk, position itself to a set of poses from any initial pose, and track a “red ball”. The fiducial marker was a red circle on a piece of paper. The robot crawled under the table by executing a finite number of crawling sequences, before moving to a sitting position. A video of this experiment was recorded for later analysis.

Following this, the optimized crawling parameters were used to generate a new gait sequence in MATLAB. The optimized and nominal gait sequences were tested using the V-REP simulator and the simulated joint torques were recorded. The V-REP simulator provides a MATLAB API to record these torques. While the optimized gait sequence was formulated using the pseduo-static assumption, the gait was tested at different speeds to compare the increase in efficiency against the nominal gait for varying degrees of dynamic loading.

Details about the crawling environments, simulation, and crawling parameters can be found in Section 5.1. Data collected about the nominal crawling experiment is presented in Section 5.2 and the optimized crawling experiment in Section 5.3.

## 5.1 Experimental Setup

The crawl gaits were tested on the Nao humanoid in the V-REP simulator using MATLAB, and by having actual robot crawl under a vertically constrained table using the NaoQI API in C++. The nominal parameters were tested both in simulation and on the actual robot, while the optimal parameters were only tested in simulation. MATLAB has tools to use genetic algorithms to optimize systems, which were used here to generate the optimal parameter splines.

### 5.1.1 Mobile Platform

The Nao humanoid was used to test the Projected Profile algorithm. Details about the Nao are discussed in Chapter II. It makes a convenient platform to test crawling algorithms as NaoQI provides an extensive API to control a range of parameters from individual joint angles to full body positioning. Importantly, the kinematic configuration of the robot is amenable to the crawling paradigm and its relatively small size allows environments to be easily constructed for testing.

### 5.1.2 Crawling Environments

Prior to any testing on the actual robot, the V-REP Simulator by Coppelia Robotics was used to verify that the algorithms functioned correctly and exhibited the desired behaviors. The V-REP simulator is a good choice for this application for a variety of reasons. It uses the mature and well known Open Dynamics Engine (ODE) as its physics simulator, supports multiple operating systems such as Windows and Linux, and provides an API for use with many languages such as C++, Python, and MATLAB. What's more, it provides a model of the Nao humanoid that can be easily commanded. Figure 22 shows an example of the Nao in V-REP set at the initial crawling position. The V-REP API also simulates various sensors, and allows the torque at each of the Nao's joints to be accessed. As mentioned in Chapter IV, this data was used to generate the gait-parameter-triplet-to-joint-torque mapping for the genetic optimizer. The simulated joint torques were also accessed while running the optimized crawling gait at different speeds to compare its improvement over the nominal gait. Results from those experiments are presented in Section 5.3.2.

While traversing rough terrain or over small obstacles is one application of a crawl gait, these experiments were instead designed to show that the robot could access areas with demanding height constraints. For this, a small table was used whose sides were

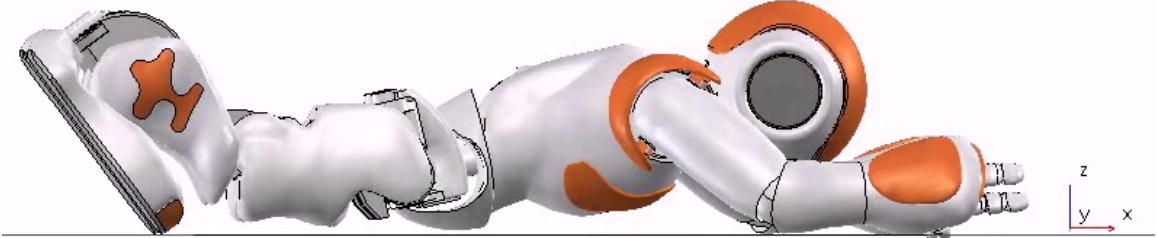


Figure 22: This figure shows the Nao humanoid V-REP simulation. The robot is positioned at the initial configuration of the close chain phase of the crawl gait.

Gait Parameter	Value
$\theta_3$	16.5°
$\theta_4$	27.5°
$\alpha$	-30° to -90°

Table 2: Table of gait parameters for the nominal crawl gait.  $\theta_3$  and  $\theta_4$  are held constant, while  $\alpha$  is linearly decreased in proportion to time.

blocked with panels down to about 200mm off of the ground. Figure 23 shows the Nao crawling under this table, with its head almost touching the bottom of the panel. This represents the practical height constraint that the Nao can satisfy with this gait.

### 5.1.3 Gait Parameters

As discussed in Chapter ??, the closed chain phase of the Projected Profile crawl gait can be parameterized on the three angles  $[\theta_3, \theta_4, \alpha]$ . These three variables are referred to as the gait parameters, or alternatively as the angle triplet. The nominal angle triplet can be seen in Table 2. They involve holding  $\theta_3$  and  $\theta_4$  constant, while varying  $\alpha$  linearly as a function of time.

Results using these nominal gait parameters can be seen in Section 5.2.

In order to optimize the gait using these parameters, the procedure outlined in Chapter ?? was used, modeling the gait parameters as cubic splines. The Genetic Algorithm in MATLAB’s Global Optimization Toolbox was used in conjunction with the V-REP torque table detailed in Chapter ?? to generate the optimal spline parameters. As the genetic algorithm cannot guarantee finding the global optima for any arbitrary function, the optimization was executed several times and the best spline parameters

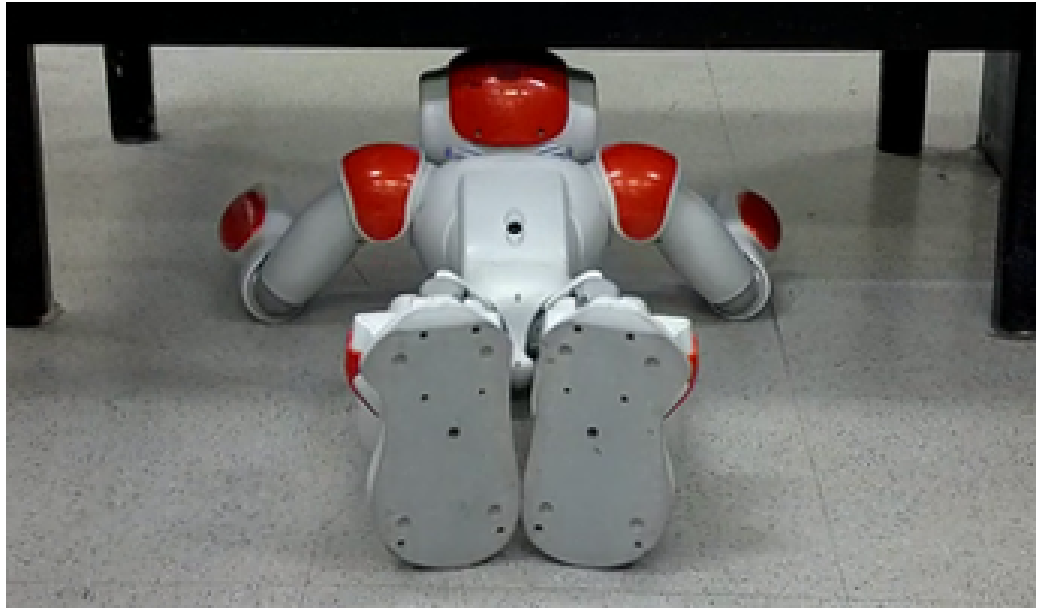


Figure 23: This figure shows the Nao as it crawls under the table with the low panels. The head of the robot can be seen to be nearly touching the panel, representing the lowest practical traversable height constraint.

were used in the experiment. Each optimization used 50 to 80 generations to converge on results, but as can be seen in Figure 24, after about 10 generations the optimization was very near the minima.

Table 3 shows the spine parameters resulting from the optimization procedure. Each gait parameter is now a cubic polynomial which is a function of time  $[\theta_3(t), \theta_4(t), \alpha(t)]$ . The coefficients from the table are used as  $c_3t^3 + c_2t^2 + c_1t + c_0$ . The  $c_0$  coefficients are simply the angles corresponding to the starting pose for the closed chain phase of the gait. The splines are also constrained to end at the final pose for the closed chain phase, which correspond to the angle triplet of  $[0.28798, 0.47997, -1.5710]$  for  $[\theta_3, \theta_4, \alpha]$ . The initial and final angle triplets are in radians.

Figure 25 shows the splines graphically, with the nominal gait parameters overlaid for comparison. While the optimized parameter trajectory for  $\alpha$  is similar to its nominal trajectory, the trajectories for  $\theta_3$  and  $\theta_4$  dip significantly, with  $\theta_4$  having the most drastic deviation from the nominal.

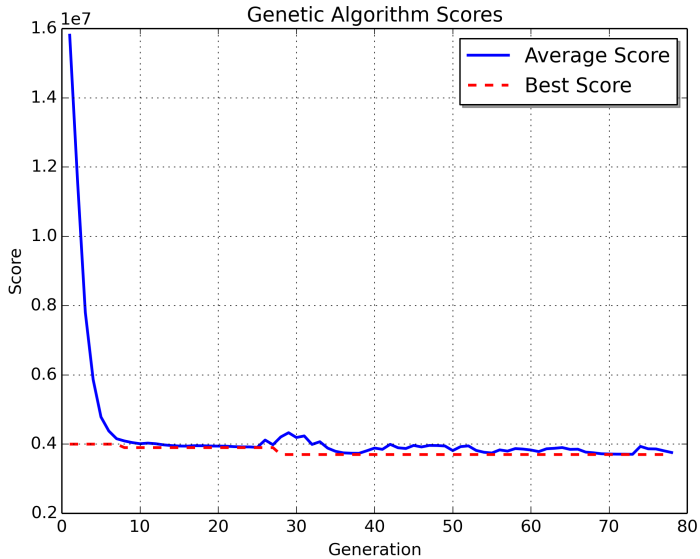


Figure 24: This figure shows one of the gait parameter optimization trials. As the genetic optimization procedure uses multiple children, the plot shows the average score for the children and the score of the best child as the generations progress.

Gait Parameter	$c_3$	$c_2$	$c_1$	$c_0$
$\theta_3$	0.2365	0.0893	-0.3267	0.28798
$\theta_4$	1.8796	-0.1365	-1.7434	0.47997
$\alpha$	-0.2134	1.1570	-1.9898	0.52360

Table 3: Table of gait parameter coefficients for the optimal crawl gait. The  $c_i$  coefficients are used in the cubic spline  $c_3t^3 + c_2t^2 + c_1t + c_0$  to vary the gait parameters as a function of time. The  $c_0$  coefficients are simply the initial starting angles for each parameter.

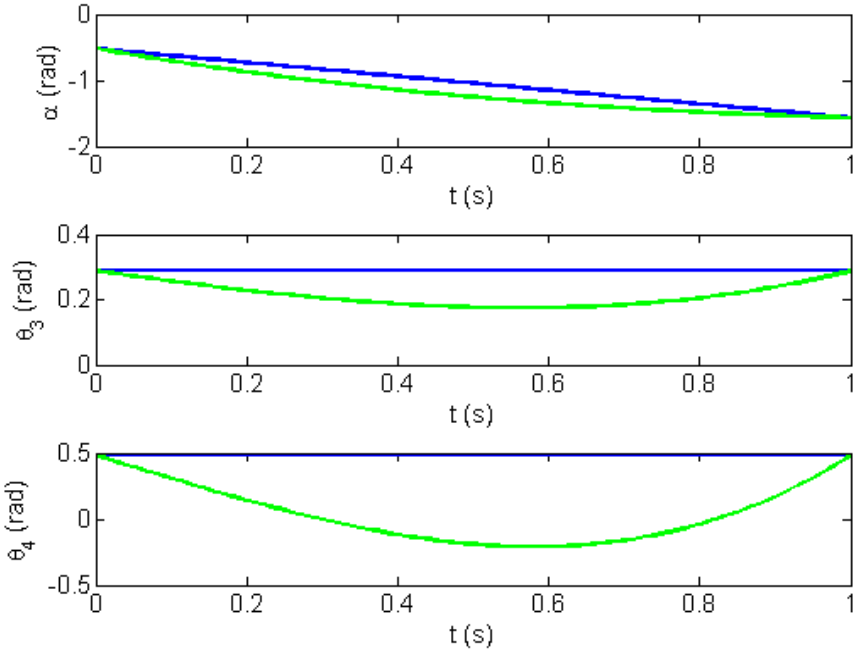


Figure 25: This figure shows the optimal gait parameter trajectories overlaid onto the nominal trajectories. The blue lines represent the nominal trajectories while the green lines show the optimal.

## 5.2 Nominal Crawl Gait Data

To test the Projected Profile gait using the nominal parameters reviewed in Section 5.1.3, the gait sequence was first generated in MATLAB and then simulated in V-REP. Following this, the gait was tested on the Nao by setting it to crawl under a vertically constrained table in two different experiments. In the first, the robot was set to the initial crawling pose and placed on the floor in front of the table. The robot then executed the crawling gait. In the second experiment the robot was programmed to recognize a fiducial marker, represented by a red circle mounted to the table, and walk to it. The robot then moved to a prone posture and crawled under the table. This procedure is more thoroughly examined in Section 5.1. Joint angle and joint motor current data was collected during the table experiments and is presented in this section. These table experiments demonstrate the efficacy of the gait to locomote the robot and the low profile nature of the gait to allow access to vertically constrained spaces.

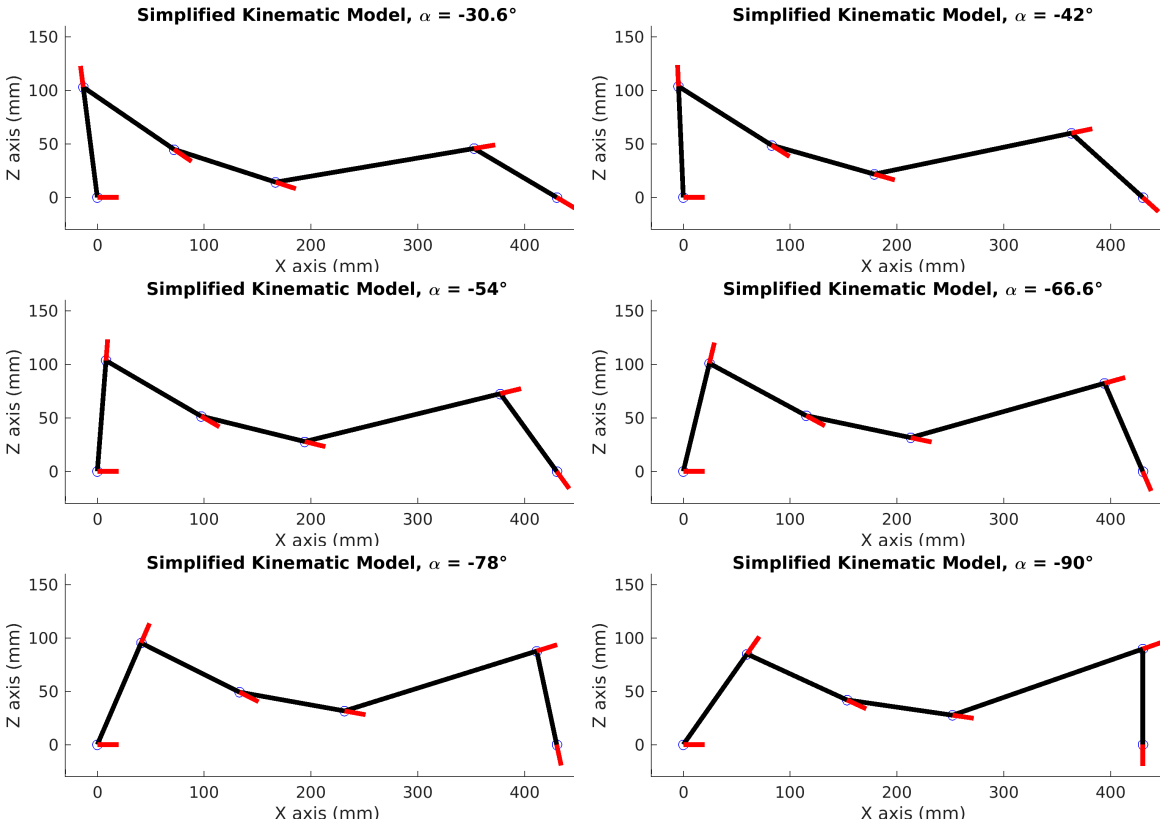


Figure 26: This figure shows a simplified kinematic model of the Nao as it executes the Projected Profile gait using nominal parameters. The model starts with  $\alpha = -30^\circ$  and terminates when  $\alpha = -90^\circ$ .

### 5.2.1 Simulations

Figure 26 shows samples of the closed chain phase of the Projected Profile gait using the nominal parameters. It shows a simplified kinematic model representing a projection of the robot onto the sagittal plane. The frames show the model starting in the initial pose, and by linearly increasing the  $\alpha$  gait parameter and holding the  $\theta_3$  and  $\theta_4$  parameters constant, the model shifts forward until  $\alpha$  has reached its terminal value. This places the model at the final closed chain pose. It can be seen that the highest point of this gait occurs at about  $z = 100 \text{ mm}$ . This model of course does not include the limb thicknesses nor the head of the Nao, as it only models joint centers. This model was created using MATLAB and is used to view the results of the gait sequence generation.

Once the gait sequence is generated, it is tested using the V-REP simulation of the Nao humanoid. Figure 27 shows the simulated Nao executing the closed chain phase of

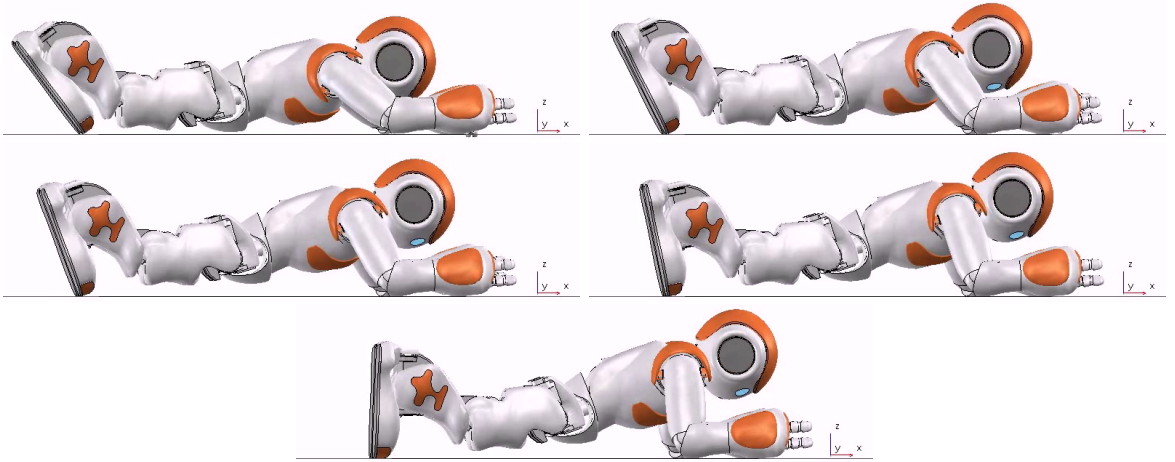


Figure 27: This figure shows the simulated Nao executing the closed chain phase of the gait using the nominal parameters.

the nominal crawl gait. As with the simplified kinematic model, the  $\alpha$  gait parameter is linearly increased from  $-30^\circ$  to  $-90^\circ$ , which moves the robot forward. As detailed in Chapter ??, the gait parameters and other constraints are used to position the arms of the robot, as unlike the ankle pitch, hip pitch, and shoulder pitch joints which have angles that directly correspond to joint angles in the simplified kinematic model, the shoulder roll, elbow yaw, and elbow roll joints do not. The head in this simulation can be seen to be the highest part of the robot throughout the majority of the gait, increasing the minimum value of the allowable vertical constraint.

### 5.2.2 Vertically Constrained Table

Following simulation, the Projected Profile crawl gait using the nominal parameters was tested on the Nao. Figure 28 shows the initial test of the robot crawling under the vertically constrained table. The Nao is set to the initial crawling pose on the floor outside of the table. The robot then executes the crawl gait for several sequences until the robot is under the table. For this experiment, the robot executed 9 sequences in 27 seconds. The robot traveled about 1 body length or 610 mm, equating to a velocity of about 22.6  $\frac{mm}{s}$ .

Figure 29 and 30 show the second experiment performed with the vertically constrained table. The robot has detected and walked to the red marker affixed to the table. It then transitions to a prone posture and begins the crawling sequence. After having crawled to the other side, the robot transitions to a sitting posture. The abil-



Figure 28: This figure shows the first experiment of the Nao crawling under the vertically constrained table.

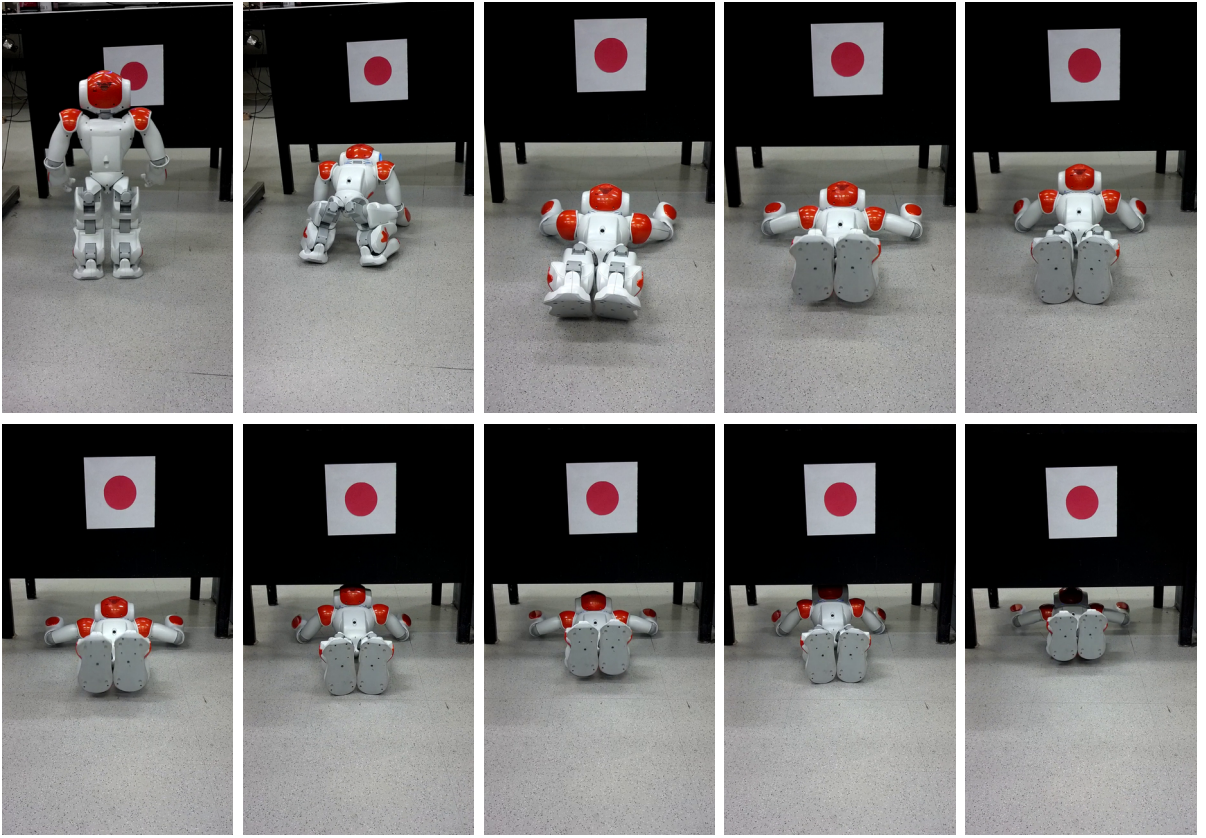


Figure 29: This figure shows the approach portion of the second vertically constrained table experiment. A red circle is used as a marker for the direction in which the robot is commanded to move. When the robot approaches below a specified distance threshold from the red circle, the crouch-down and crawl gait sequence is initiated.

ity to transition from posture to posture is provided through the NaoQI API. For this experiment, the robot executed 25 sequences in 58 seconds. The robot traveled about 2.75 body lengths or  $1,676.4 \text{ mm}$ , equating to a velocity of about  $28.9 \frac{\text{mm}}{\text{s}}$ .

### 5.2.3 Joint Data

The NaoQI API provides functions for recording joint angles and motor currents. During the nominal crawl gait experiments, these values were recorded and Figures 31, 32, and 33 plot the results. Figure 31 plots the joint angles for the arms and legs of the robot during the execution of multiple gait cycles. As expected, the plots show a clear periodicity to the gait. As the gait is laterally symmetric, the joint angles for the left and right side of the robot are the similar, with the exception of the arm joints below the shoulder pitch. Due to the robot frame and joint frame definitions from the NaoQI

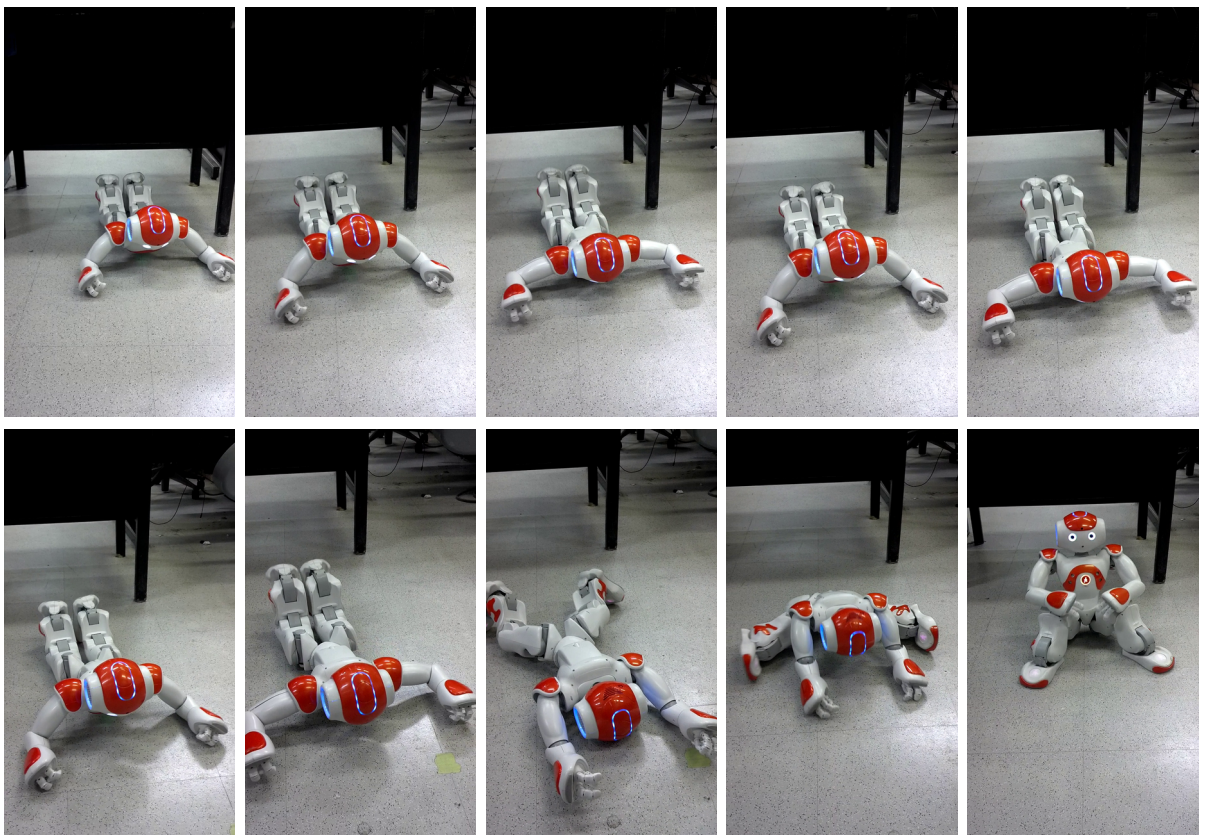


Figure 30: This figure shows the recovery portion of the second vertically constrained table experiment. After the Nao has executed a set number of crawl sequences, the robot transitions to a sitting posture.

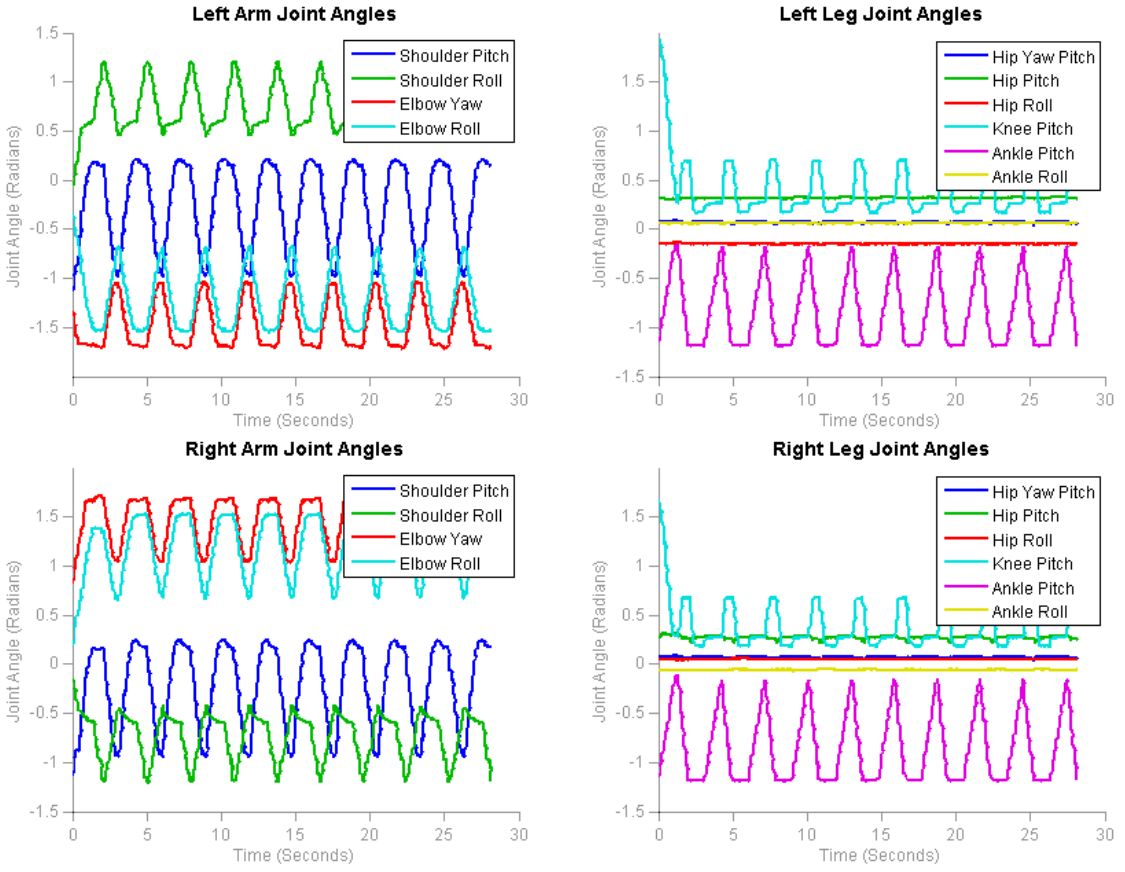


Figure 31: This figure shows the measured joint angles during multiple iterations of the periodic crawling gait. The angles for the left and right side can be seen to be identical, except for those of the shoulder roll, elbow yaw, and elbow roll. These have a mirror symmetry, due to the joint frame definitions.

API, the shoulder roll, elbow yaw, and elbow roll have a mirror symmetry rather than being identical. Figure ?? details the joint frame definitions. In addition, the hip yaw pitch, hip roll, and ankle roll are not symmetric here as they were set to small constants that do not actively participate in the Projected Profile gait.

Figure 32 shows the full joint angle sequence as the robot transitions from standing to crawling. The Nao starts in a standing posture and then transitions to a crouch posture. From there, it transitions to the initial crawling pose and begins to crawl. It executes five crawl sequences to simulate crawling under an object. Only five sequences were performed in order to make the plot of the joint angles easier to present. The robot then transitions back to the crouching posture. Each of the posture transitions was executed using the NaoQI ALRobotPosture API. Figure ?? shows the different

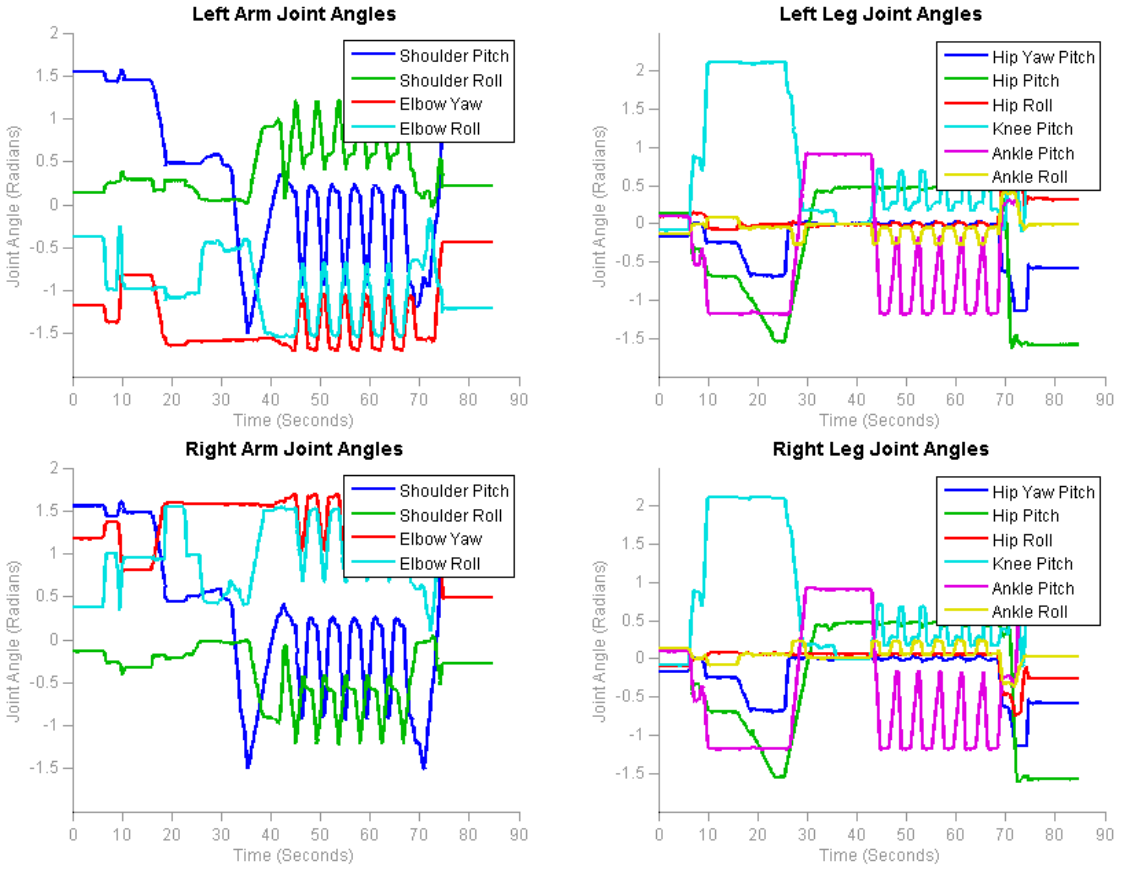


Figure 32: Measured joint angles for a sequence of transitioning from standing to crouch to crawling, crawling under a table, and then returning to crouch.

postures used in these transitions.

While the Nao platform is equipped with encoders that can directly measure joint angle, it is not equipped with joint torque sensors. The robot is equipped with sensors that measure joint motor current which can be used to estimate joint torque. The motor currents were recorded for several crawl sequences and are presented in Figure 33. While the plots do show a periodicity to the motor current draws, it is difficult to observe other useful information. Though there is a relationship between motor current and joint torque, in general, current sensors give a poor estimate of torque. One limiting factor is that each joint uses some form of motor control to bring the joint to a desired angle. This controller will obfuscate the torque-current relationship as it draws power to position the joint. Therefore, the joint current plots are of limited use.

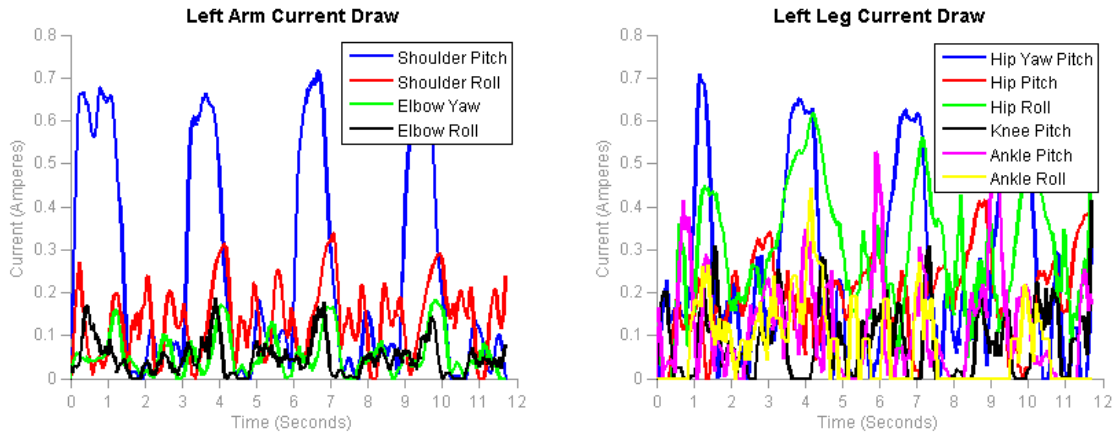


Figure 33: Measured motor current draws during multiple iterations of the periodic crawling gait.

### 5.3 Optimized Crawl Gait Data

To test the Projected Profile gait using the optimal parameters reviewed in Section 5.1.3, the gait sequence was generated in MATLAB and simulated in V-REP. The closed chain phase of the gait was the only portion that was optimized, so that phase of the gait was simulated and analyzed. As reviewed in Section 5.1.2, the V-REP simulator provides joint torque simulation and sensing, which can be recorded to evaluate the increase in gait efficiency using these parameters.

#### 5.3.1 Simulations

Figure 34 shows samples of the simplified kinematic model, as it executes the closed chain phase of the optimized Projected Profile gait. As with the nominal crawl gait, the angle  $\alpha$  transits from  $-30^\circ$  to  $-90^\circ$ , though not linearly, as reviewed in Section 5.1.3. While it is difficult to see the difference in the optimized  $\alpha$  trajectory from the nominal version, the trajectory of  $\theta_3$  and  $\theta_4$  are quite different from those seen in Figure 26. As opposed to the nominal gait which appears to hold the midsection of the model low to the ground, the optimized gait arches the midsection upwards as the gait progresses, before being brought down. This resembles the tendency for humans to arch their back when attempting to support their weight in similar positions.

The V-REP simulation of the Nao executing the optimized gait can be seen in Figure ???. As with the simplified kinematic model, the Nao can be seen to be using its hips and knees to arch its back during the gait sequence.

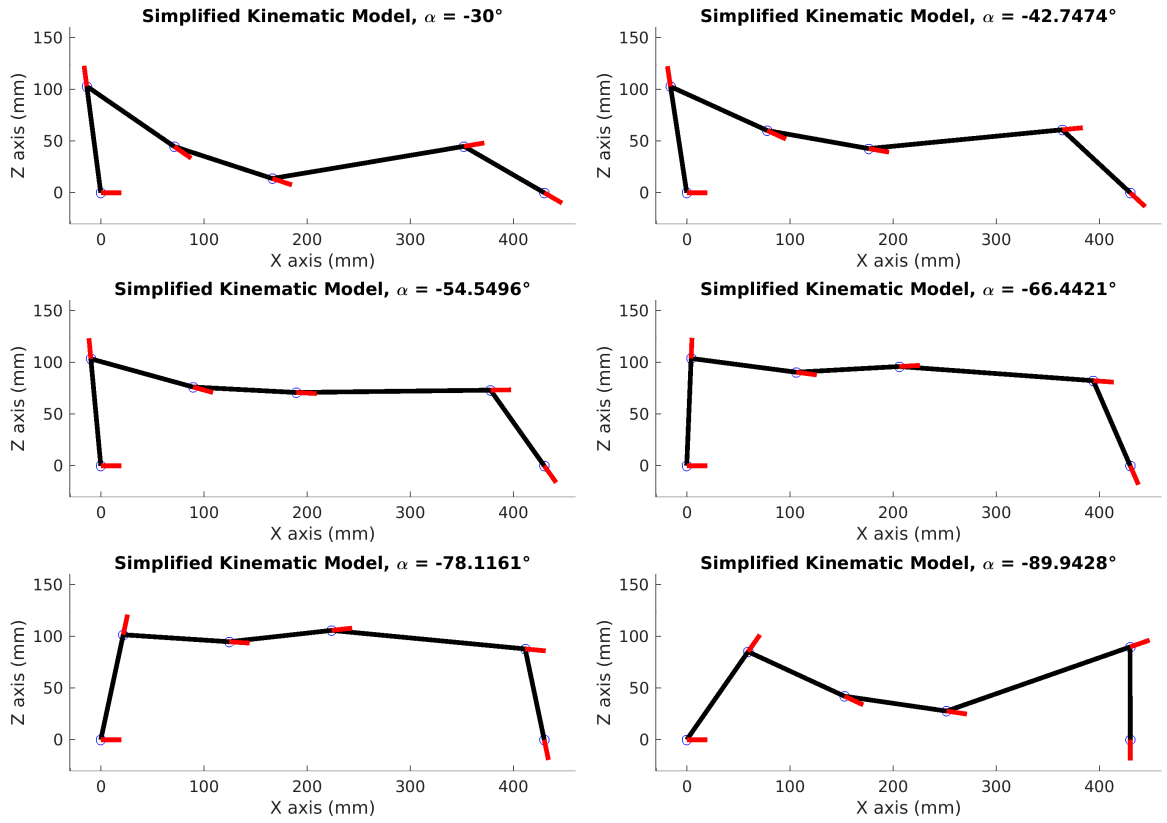


Figure 34: This figure shows the simplified kinematic model executing the close chain phase of the optimized gait.

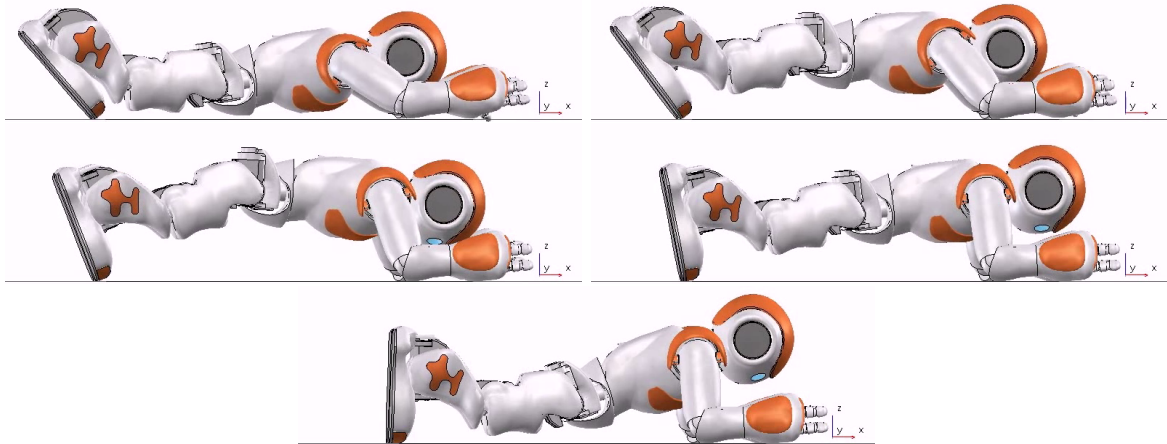


Figure 35: This figure shows the simulated Nao executing the closed chain phase of the optimized gait.

### 5.3.2 Joint Torque Data

In order to analyze the efficiency increase to the gait using the optimal gait parameters, the torques from the simulated Nao were recorded during nominal and optimal closed chain phase gait executions. The simulated torques are easier to interpret than the motor currents presented in Section 5.2.3 as they directly represent the torques the Nao would experience during a crawl. The ankle pitch, knee pitch, hip pitch, and shoulder pitch torques of the simulated Nao were recorded, corresponding to the Projected Profile joints  $[\theta_2, \theta_3, \theta_4, \theta_5]$ . These were the joints which were used in the optimization procedure and were therefore recorded for analysis. To test the efficacy of the pseudo-static assumption, the crawl gaits were executed at different speeds so that the effects of transient torques would be present to varying degrees. As discussed in Chapter ??, the pseudo-static model assumes that gravity is the dominant force in the system and the transients do not affect the system significantly. Ten speeds were tested for each gait. The duration of each closed chain gait phase varied from one second to ten seconds, in one second increments. The transient torques will have a stronger influence on the joint torques at the higher speeds.

Figures 36 and 37 show joint torque plots from the nominal and optimal gaits, respectively. Each panel shows the torques for each of the four joints, over the prescribed gait duration. Only a subset of the experiments are shown as the differences between panels diminishes as the duration increases. This is likely due to a shift from the dominant component of the system being the transient torques to the pseudo-statics.

Figures 38 and 39 overlay the torques onto each other which shows their similarity during the initial portion of the gait, before fanning out in the later portion. The panels show the torque curves for each joint as a function of time. This similarity is demonstrated more clearly in Figures 40 and 41, which highlight the transients. For the nominal gait, the joint torque curves for each joint from about  $t = 0.0$  seconds to  $t = 0.25$  seconds are similar regardless of the gait duration. The optimal gait has a similar time interval at around  $t = 0.0$  seconds to  $t = 0.175$  seconds. After these points, as seen in Figures 38 and 39, the curves tend to diverge. This gait-duration-invariant-with-respect-to-time portion suggests that the system transients are the dominant forces in this region. For the shorter duration gaits, this means the transients dominate as much as 20% of the gait cycle. But as the gait cycle duration is increased, the transients contribute to a diminishing percentage of the gait cycle, which appears as the left most

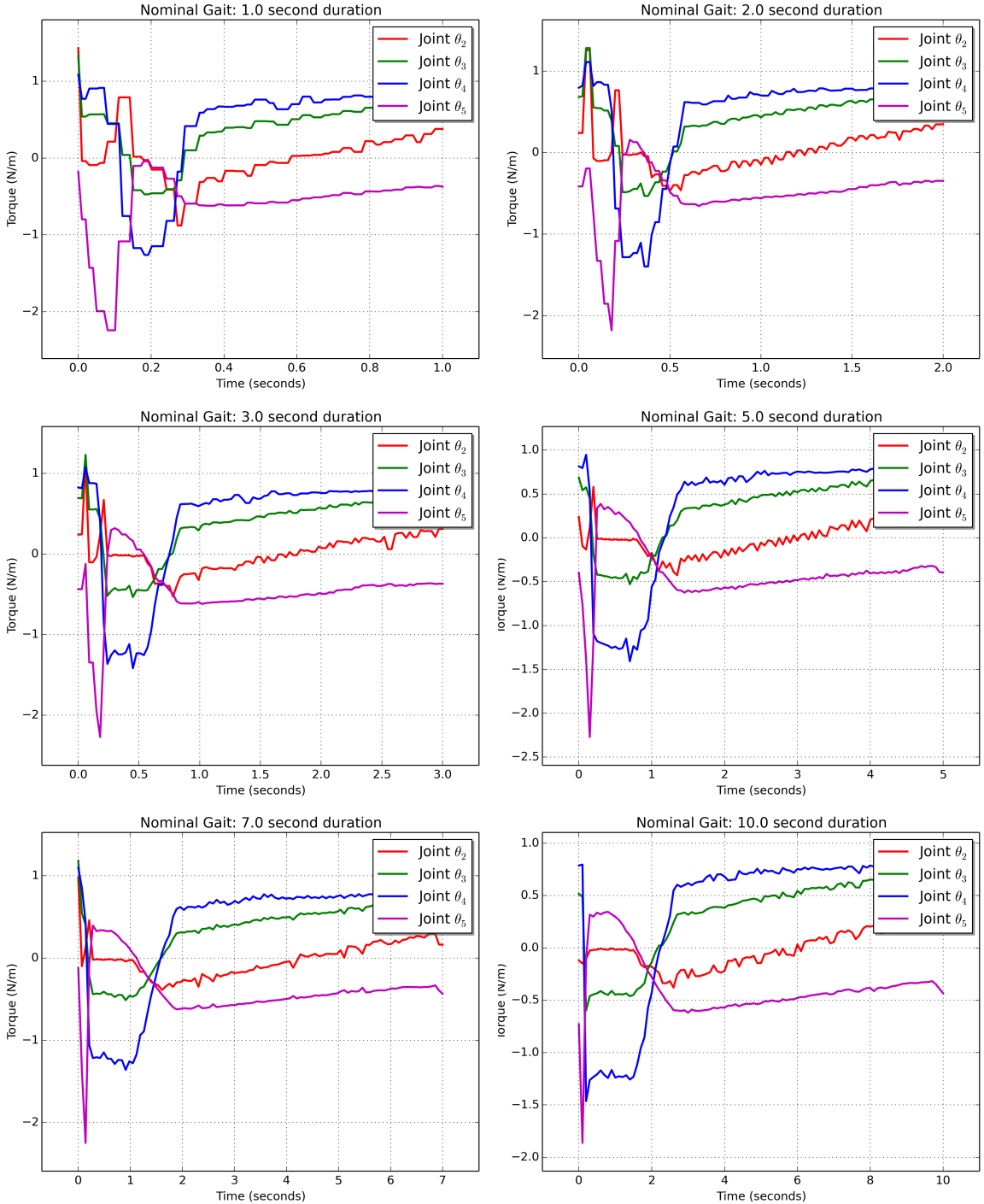


Figure 36: This figure shows the nominal joint torque curves for six durations. As the durations are increased, the graphs can be seen to be increasingly similar.

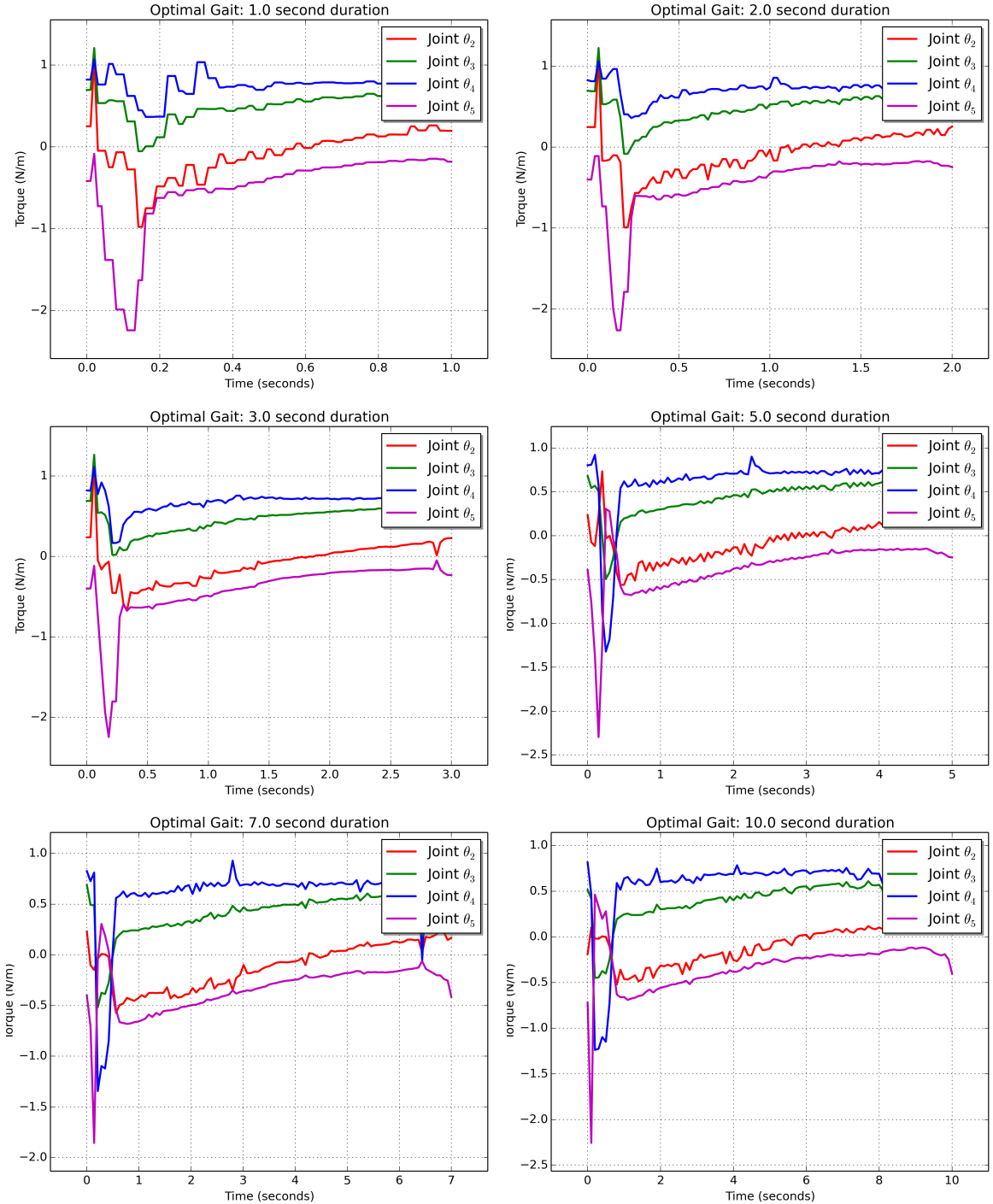


Figure 37: This figure shows the optimal joint torque curves for six durations. As the durations are increased, the graphs can be seen to be increasingly similar.

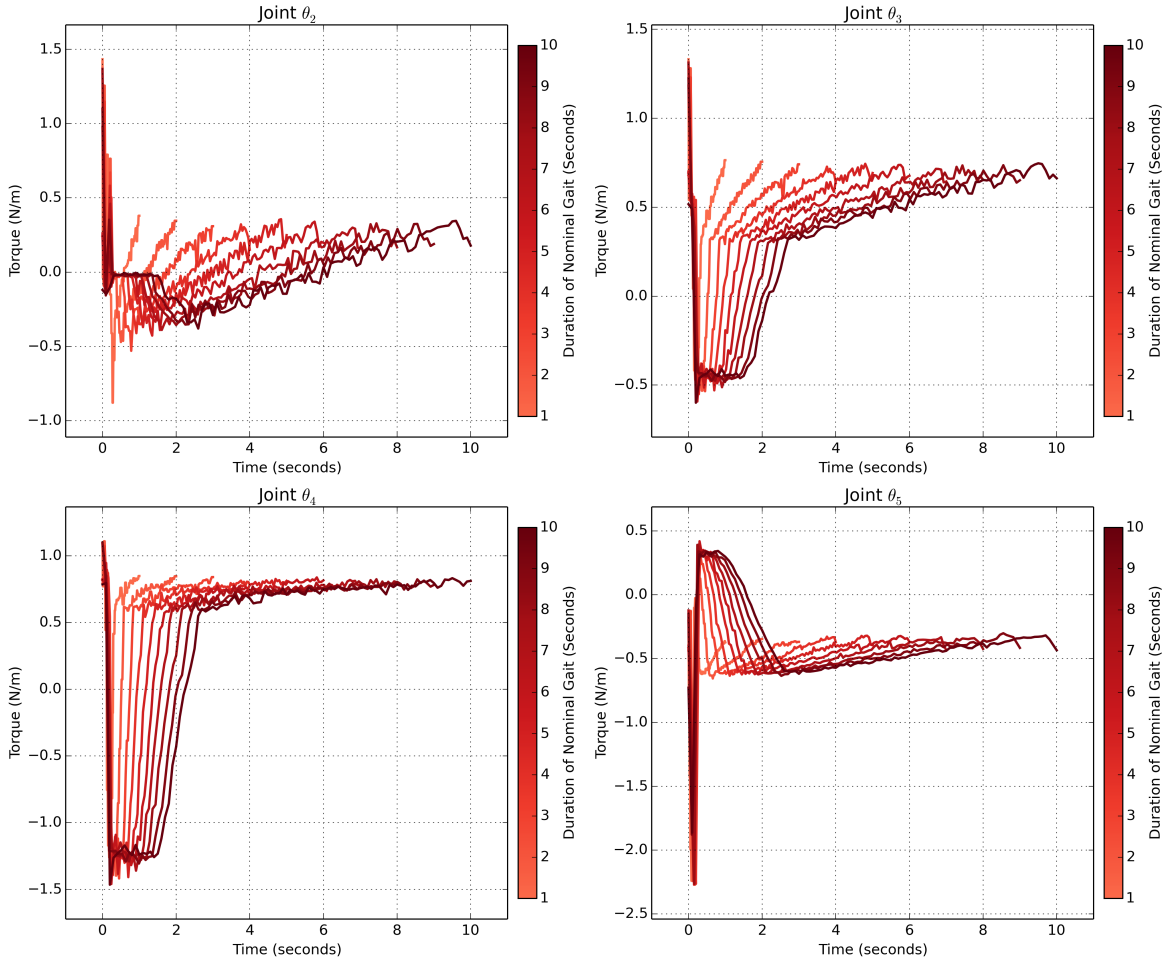


Figure 38: This figure shows the nominal joint torque curves as a function of time. Each panel shows the curves for one joint. The curves can be seen to be similar up to a certain time, at which point they diverge.

portion of the panels in Figures 36 and 37 being compressed to the left. The differences between the 7 second gait and the 10 second gait for example, are less pronounced than between the 1 and 3 second gaits.

This similarity is more clearly demonstrated in Figures 42 and 43. These panels plot joint torques for each joint as a function of gait cycle percentage, rather than time. Within each of the panels, the joint torques from the percentage from 20% to 100% can be seen to be similar. This gait-duration-invariant-with-respect-to-cycle-percentage portion suggests that the pseudo-statics are the dominant forces in this region. This is because joint torques are now only a function of position and not the time it takes to get to that position.

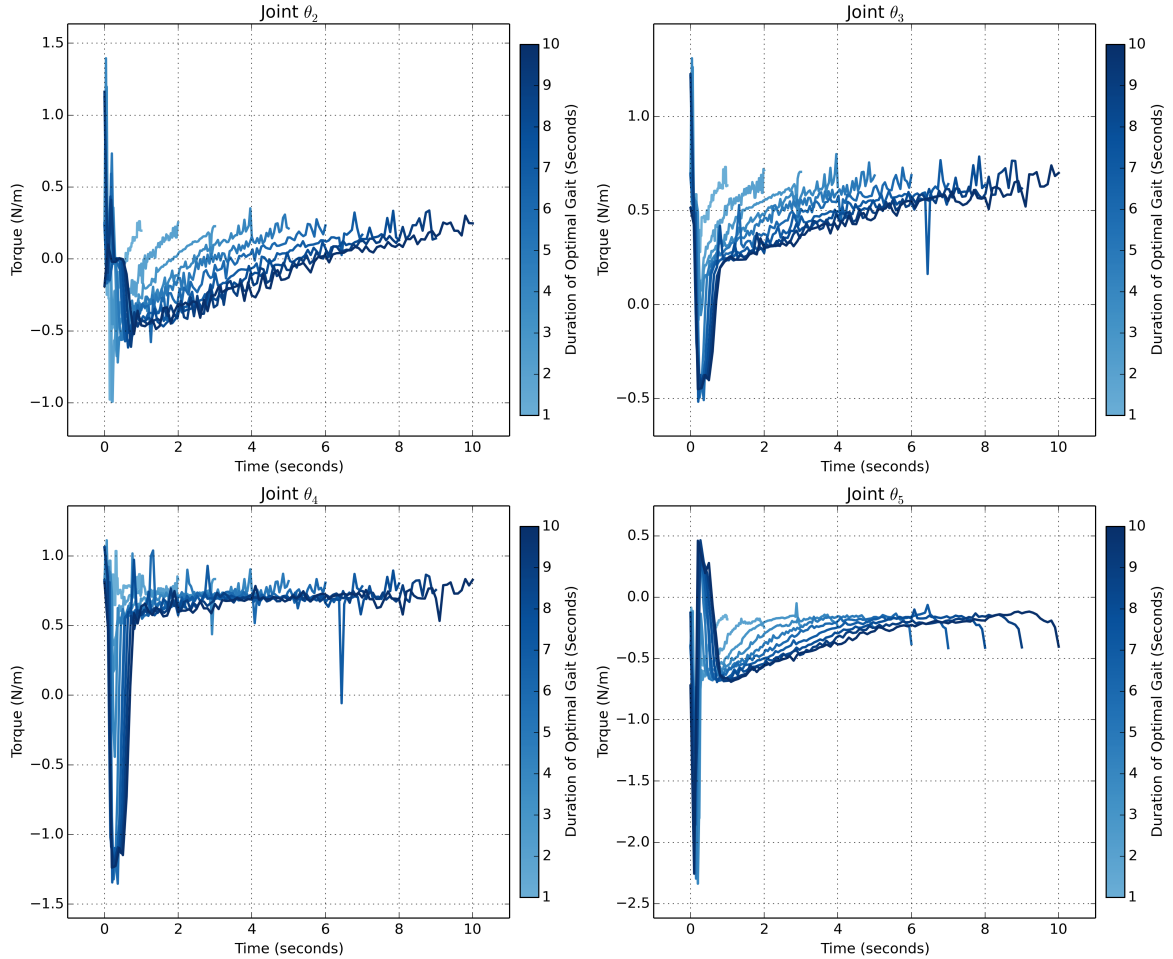


Figure 39: This figure shows the optimal joint torque curves as a function of time. Each panel shows the curves for one joint. The curves can be seen to be similar up to a certain time, at which point they diverge.

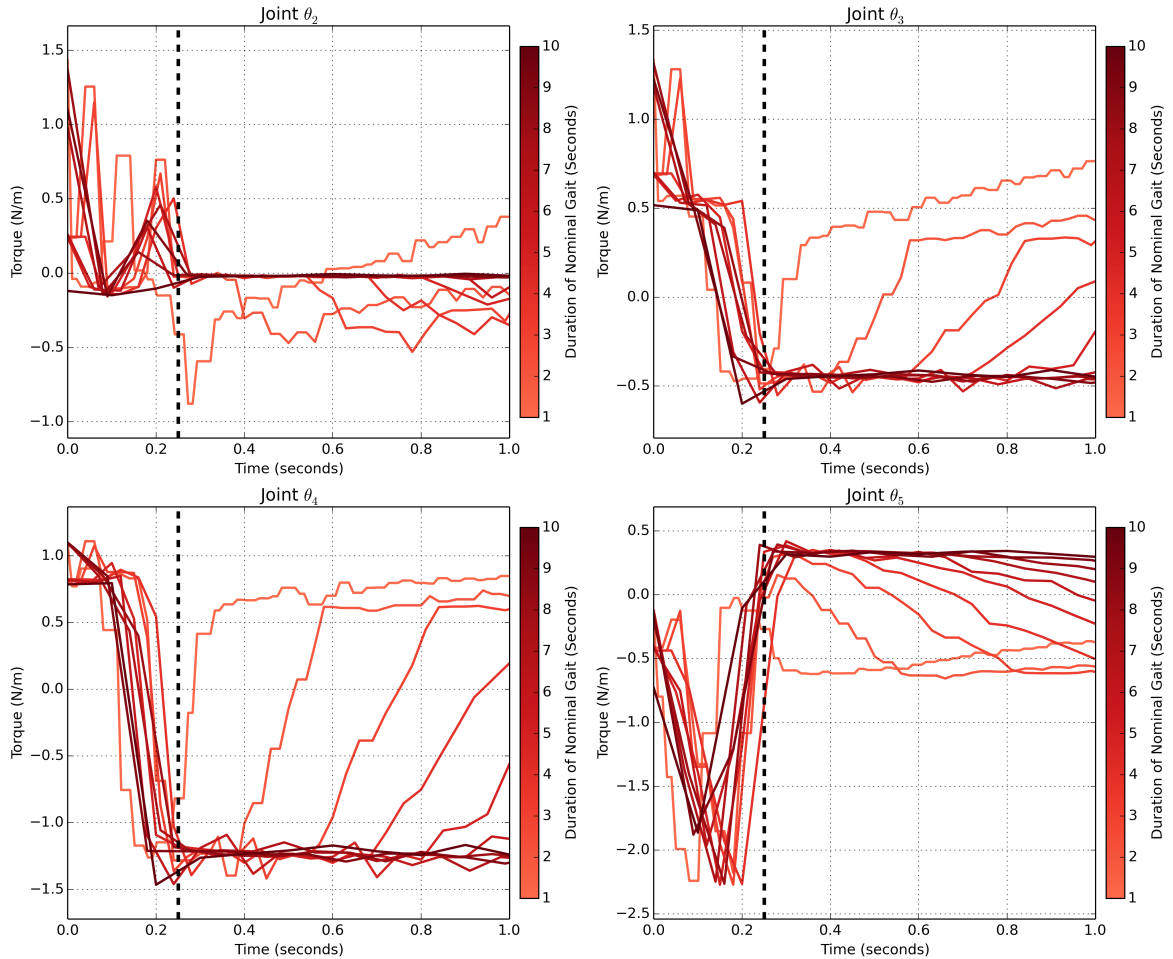


Figure 40: This figure shows a magnified view of the nominal joint torque curves as a function of time. Each panel shows the curves for one joint. The curves are overlaid to show their similarities when viewed with respect to time. The dashed black line signifies the time at which the curves diverge.

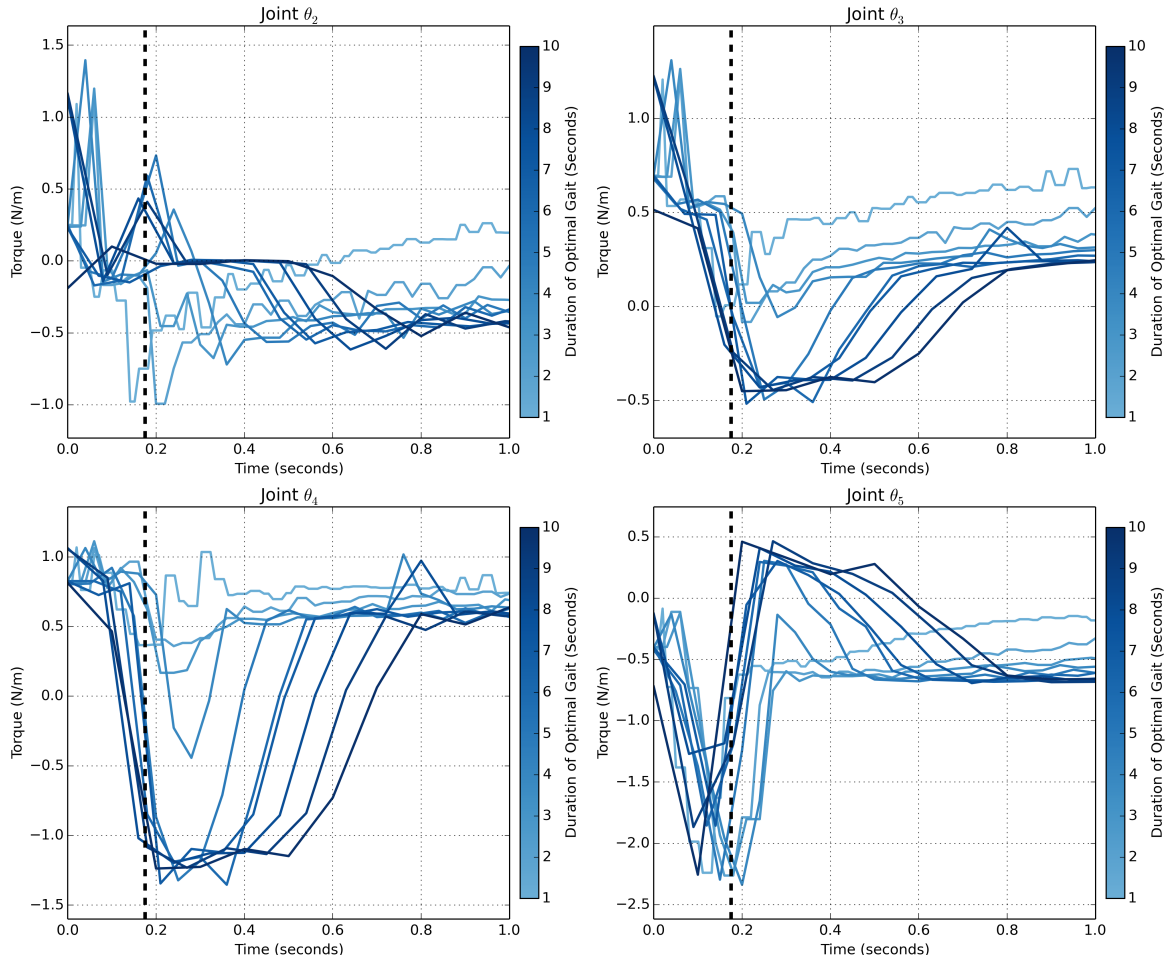


Figure 41: This figure shows a magnified view of the optimal joint torque curves as a function of time. Each panel shows the curves for one joint. The curves are overlaid to show their similarities when viewed with respect to time. The dashed black line signifies the time at which the curves diverge.

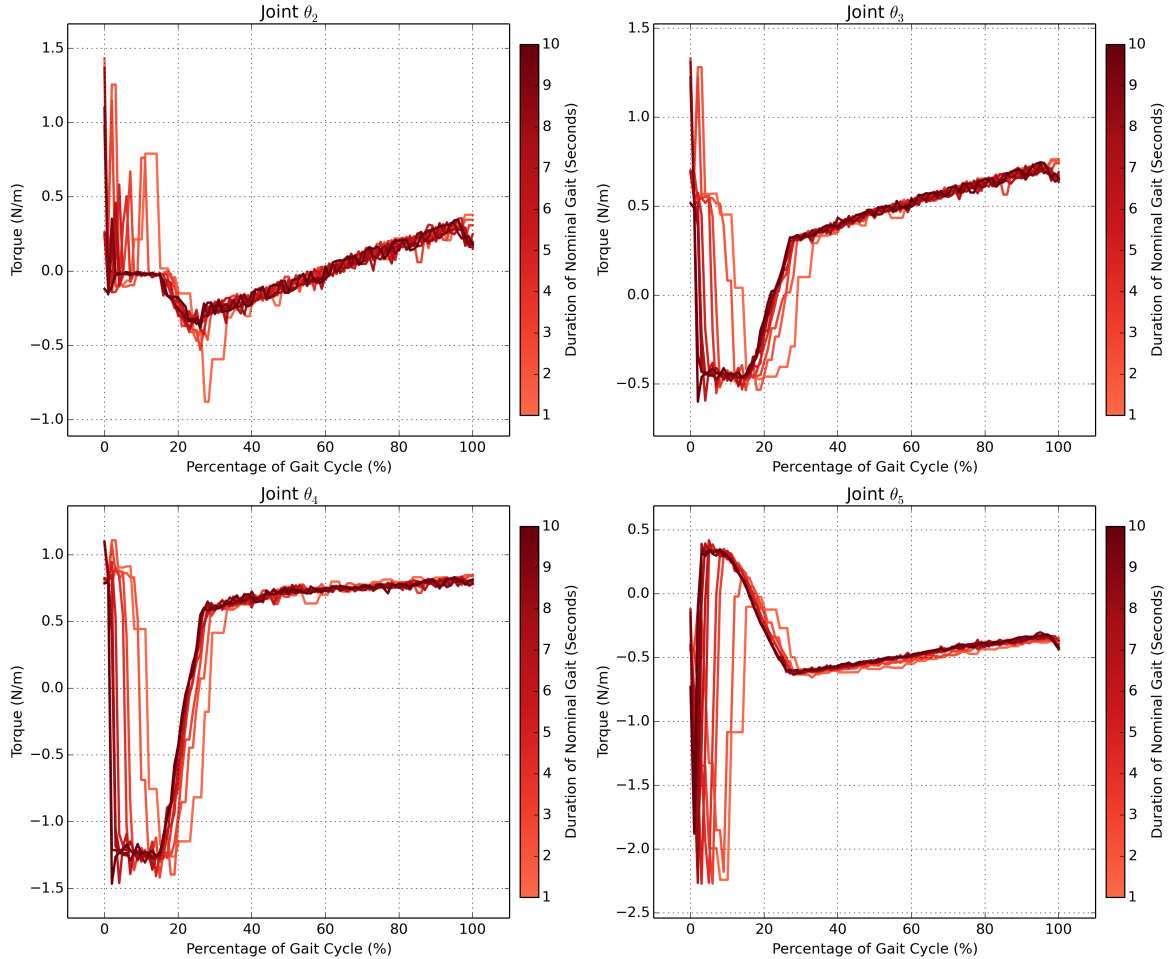


Figure 42: This figure shows the nominal joint torque curves as a function of gait cycle percentage. Each panel shows the curves for one joint. The curves are overlaid to show their similarities when viewed with respect to cycle percentage.

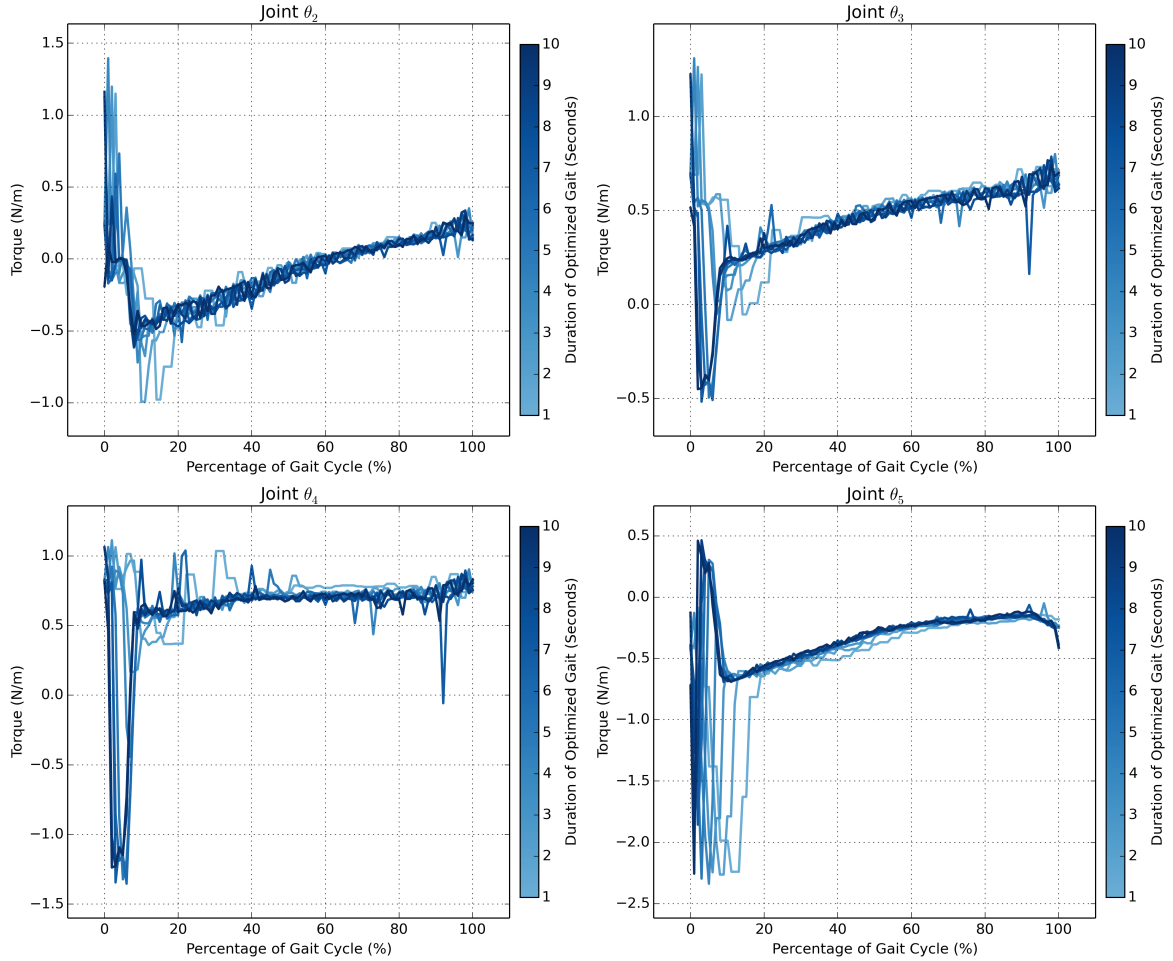


Figure 43: This figure shows the optimal joint torque curves as a function of gait cycle percentage. Each panel shows the curves for one joint. The curves are overlaid to show their similarities when viewed with respect to cycle percentage.

When comparing the nominal gait torque curves to the optimal ones, as in Figure 44, a number of effects can be seen. For short duration gaits where the transient dynamics are dominant, a pattern is less obvious though the amplitude of the torque transients for joints  $\theta_3$  and  $\theta_4$  have been reduced. In the Nao, these are the knee pitch and hip pitch joints. In the longer duration gaits, the optimization appears to have the effect of compressing the transients to the left and reaching the affine region of the torque curve more quickly. This means while the torque curves do transit through these higher magnitude regions, they spend less time there and therefore accrue a lower torque cost.

Examining the torque costs of the two gaits as a function of duration in Figure 45 supports the idea that as the effects of the transients diminishes and the pseduo-statics become more dominant, the efficacy of the optimization increases. This is expected as the optimization was formulated with this assumption. It should be noted that the costs presented in Figure 45 are not weighted according to the weight vector presented in Chapter 4.3.2. The figure shows the integral of the costs with the weight vector  $w = [1, 1, 1, 1]^T$  in order to show the simple torque cost to the robot. The absolute and percentage difference in costs for the short durations is small, though the optimal gait always outperforms the nominal gait. As the durations increase, the optimal gait uses up to 21.5% less than the nominal gait. Therefore, while the optimal gait does not always outperform the nominal gait by a significant amount, it is always preferable to the nominal gait.

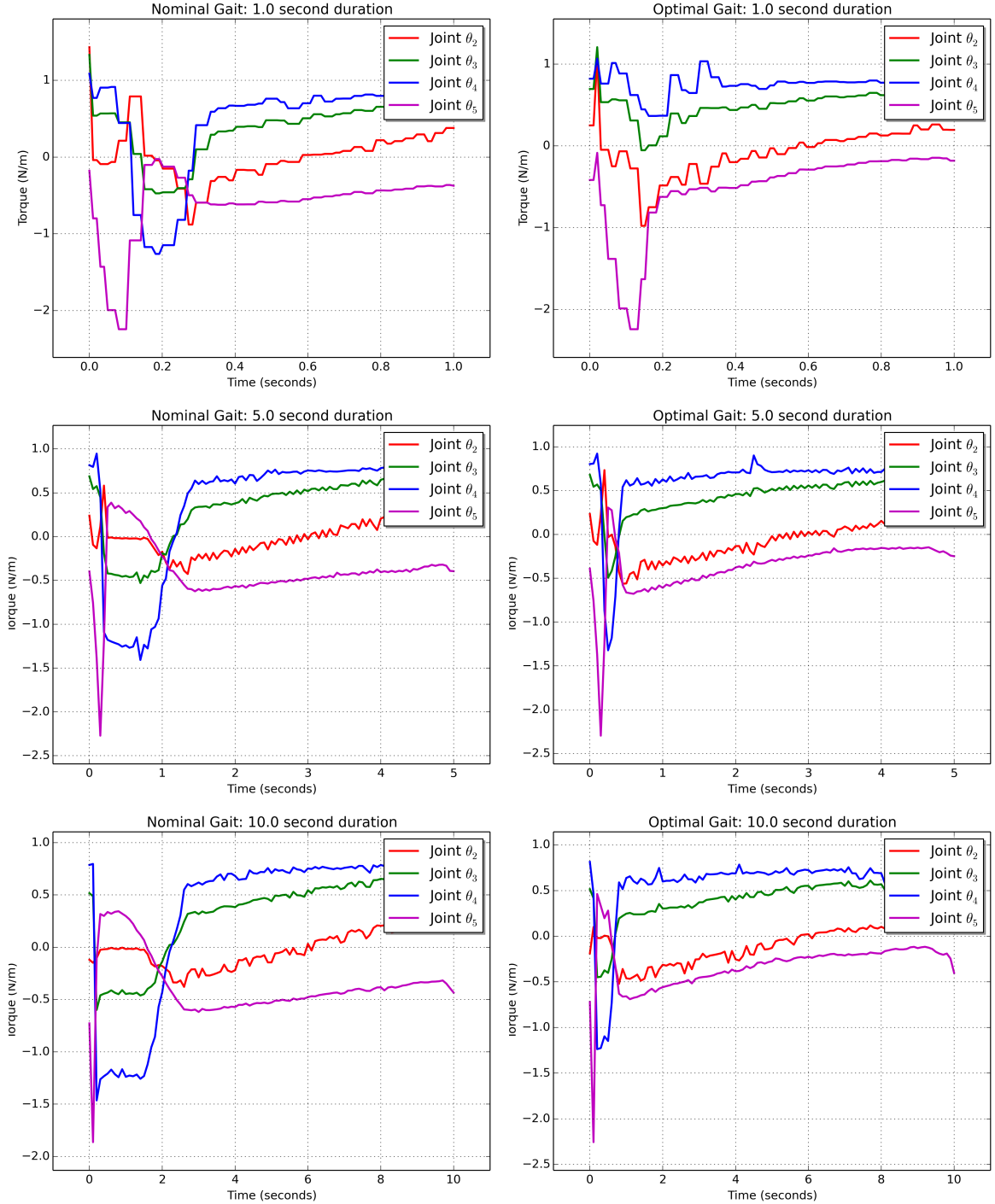


Figure 44: This figure compares the joint torque curves of the nominal and optimal gaits for three gait durations. The optimal curves appear to be extending the affine portion to the left, reducing the transient response.

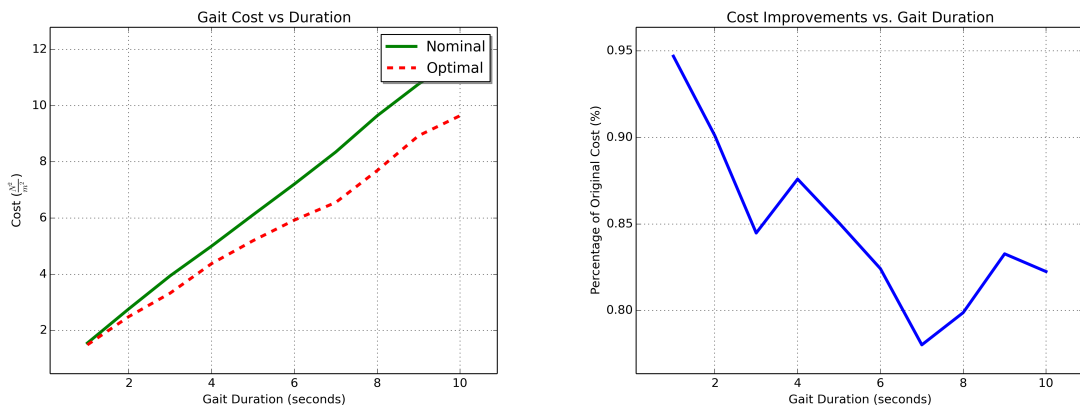


Figure 45: This figure shows the cost comparisons between the optimal and nominal gaits as a function of gait duration. The left panel shows this in terms of absolute cost and the right panel shows this in terms of percentage. The right panel percentage is the ratio of the optimal gait cost to the nominal gait cost for each duration  $\frac{C_o}{C_n}$ .